PHYSICAL REVIEW A VOLUME 36, NUMBER 4 AUGUST 15, 1987

Schwinger multichannel study of the $^2\Pi_g$ shape resonance in N_2

Winifred M. Huo*
Radiation Laboratory, University of Notre Dame, Notre Dame, Indiana 46556

Thomas L. Gibson,† Marco A. P. Lima,‡ and Vincent McKoy
Arthur Amos Noyes Laboratory of Chemical Physics, California Institute of Technology, Pasadena, California 91125
(Received 24 February 1987)

We report the results of a study on electron-target correlations in the $^2\Pi_g$ shape resonance of elastic e-N_2 scattering, using the Schwinger multichannel formulation. The effects of basis set, orbital representation, and closed-channel configurations are delineated. The different roles of radial and angular correlations are compared. Our results are in good agreement with a recent calculation by Schneider and Collins [Phys. Rev. A **30**, 95 (1984)] using the linear algebraic-optical potential method whereas calculations using radial correlations alone agree well with previous calculations based on a variety of different approaches.

I. INTRODUCTION

Low-energy electron-molecule collisions play an important role in the reentry physics for the next generation of space vehicles as well as in the modeling of planetary atmospheres, gas lasers, plasma etching, and swarm processes. Among such systems, the $^2\Pi_g$ channel of N_2 has received much attention as a result of its role in the vibrational excitation of N_2 by electron impact. Experimental and theoretical studies on this resonance have been reviewed by Schulz,[1] Trajmar *et al.*,[2] and Lane.[3] The first *ab initio* determination of the width of the shape resonance near 2.3 eV was carried out by Schneider *et al.*[4] using the R-matrix method. Width calculations have also been carried out by Hazi and co-workers[5,6] using the Stieltjes imaging technique. More recent R-matrix calculations include the work of Burke *et al.*,[7] Le Dourneuf *et al.*,[8] and Morgan.[9] In addition, this channel has been studied using an iterative close-coupling method,[10] a many-body optical-potential approach,[11] a noniterative partial-differential-equation method,[12,13] a linear algebraic method,[14,15] a complex coordinate self-consistent-field (SCF) technique,[16] as well as a standard bound-state configuration-interaction (CI) method with noninteger nuclear charges.[17,18] The importance of electron correlation (polarization) is amply demonstrated in these calculations.

The Schwinger multichannel (SMC) formulation[19,20] is a general method for the calculation of elastic and electronically inelastic electron-molecule collision cross sections at low and intermediate energies, with targets of arbitrary symmetry. It has been successfully applied to the treatment of elastic scattering by H_2, CH_4, and H_2O.[21–23] It has also been applied to the study of the electron impact excitation of H_2.[24] In this paper, we apply this formulation to the study of the $^2\Pi_g$ resonance in low-energy e-N_2 scattering. The purpose of this study is twofold. First, it represents the initial application of this formulation to a study of a shape resonance. While our previous study of the e-H_2 system[21] demonstrated that polarization can be treated reliably by the SMC method, the important effects in that system are due to angular correlations.[15] On the other hand, radial correlations dominate in the $^2\Pi_g$ resonance in N_2. It is of interest to test how well this kind of correlation can be treated in the SMC method. Secondly, in the design of the next generation of space vehicles, the modeling of the flow field upon their reentry into the earth's atmosphere requires the knowledge of elastic and inelastic collision cross sections between low-energy electrons and rovibrationally hot molecules. Due to the difficulty in preparing targets at high rovibrational temperatures, such data are not available experimentally. The SMC formulation is well suited to provide such data. There are no additional computational difficulties in the method when the molecule is near dissociation. Also, since the method can treat both elastic and inelastic collisions, certain computational economies can in principle be achieved.

In this paper, we report the results of our study on the $^2\Pi_g$ channel in elastic e-N_2 scattering. The results from other partial-wave channels as well as the integral and differential elastic cross sections will be presented in a companion paper referred to below as II.[25] A report on the calculations of vibrational excitation cross sections of rovibrationally hot N_2 based on the widths deduced from the present work has been published elsewhere.[26] A brief review of the SMC formulation is provided in Sec. II. In Sec. III, the applicability of the generalized optical theorem in the SMC formulation and its relationship to the unitarity of the S matrix are discussed. The computational details are given in Sec. IV. Particular attention is paid to the choice of the insertion basis set used in the separable L^2-representation of the free-particle Green's function and to the choice of closed-channel configurations to represent polarization effects. Our results are presented in Sec. V and Sec. VI summarizes our conclusions.

II. SCHWINGER MULTICHANNEL VARIATIONAL METHOD

The Schwinger multichannel formulation has been discussed previously.[19,20] Here we give a brief review of the working equations only. Let $\Psi_n^{(+)}$ be the total $(N+1)$-particle antisymmetrized wave function with incoming plane wave and outgoing wave boundary conditions for the nth channel. A projected Lippman-Schwinger equation for $\Psi_n^{(+)}$ is

$$P\Psi_n^{(+)}=S_n+G_P^{(+)}V\Psi_n^{(+)} . \tag{1}$$

The projection operator P defines the open-channel space in terms of the eigenfunctions Φ_m of the target Hamiltonian H_N,

$$P=\sum_{m=1}^{M} |\Phi_m(1,2,\ldots,N)\rangle\langle\Phi_m(1,2,\ldots,N)| , \tag{2}$$

and

$$H_N|\Phi_M\rangle=E_m|\Phi\rangle . \tag{3}$$

The open channels are associated with those target states with energy E_m less than $\mathcal{E}$, the total energy of the electron + molecule system. In Eq. (2) P is defined in the N-electron space instead of the $(N+1)$-electron space as in the Feshbach formalism.[27] In Eq. (1), S_n is the solution of the unperturbed Hamiltonian, H_N+T_{N+1}, and is given by[28]

$$S_n=\left[\frac{k_n}{(2\pi)^3}\right]^{1/2}\exp(i\mathbf{k}_n\cdot\mathbf{r}_{N+1})\Phi_n . \tag{4}$$

The interaction potential V between the incident electron and the target is

$$V=\sum_{i=1}^{N}\frac{1}{|\mathbf{r}_i-\mathbf{r}_{N+1}|}-\sum_{\alpha}\frac{Z_\alpha}{|\mathbf{R}_\alpha-\mathbf{r}_{N+1}|} . \tag{5}$$

The projected outgoing-wave Green's function $G_P^{(+)}$, defined in the open-channel space, is given by

$$G_P^{(+)}=-\frac{1}{2\pi}\sum_{m}^{M}|\Phi_m\rangle\frac{\exp(ik_m|\mathbf{r}_{N+1}-\mathbf{r}'_{N+1}|)}{|\mathbf{r}_{N+1}-\mathbf{r}'_{N+1}|}\langle\Phi_m| . \tag{6}$$

To define a complete equation for Ψ_n, we must recover the unprojected component of Eq. (1). This is accomplished by the requirement that $\Psi_n^{(+)}$ satisfies the Schrödinger equation as well as the projected Lippmann-Schwinger equation:

$$\hat{H}\Psi_n^{(+)}=\hat{H}[\alpha P\Psi_n^{(+)}+(1-\alpha P)\Psi_n^{(+)}]=0 , \tag{7}$$

where $\hat{H}=\mathcal{E}-H_{N+1}$ and α is a parameter chosen to give a variationally stable scattering amplitude. The above equation introduces the closed channels without defining the closed-channel Green's function, which would require the inclusion of the target continuum states. As shown by Takatsuka and McKoy,[19,20] a complete equation for $\Psi_n^{(+)}$ is given by

$$A^{(+)}\Psi_n^{(+)}=VS_n , \tag{8}$$

with

$$A^{(+)}=\tfrac{1}{2}(PV+VP)-VG_P^{(+)}V+\frac{1}{N+1}\left[\hat{H}-\frac{N+1}{2}(P\hat{H}+\hat{H}P)\right] . \tag{9}$$

Based on Eq. (8), a variational expression for the fixed-nuclei T matrix is

$$T_{mn}=\frac{\langle S_m|V|\Psi_n^{(+)}\rangle\langle\Psi_m^{(-)}|V|S_n\rangle}{\langle\Psi_m^{(-)}|A^{(+)}|\Psi_n^{(+)}\rangle} . \tag{10}$$

The above quantity is calculated in the molecular frame[3] using the fixed-nuclei approximation.

III. APPLICABILITY OF THE GENERALIZED OPTICAL THEOREM AND THE UNITARITY OF THE S MATRIX IN THE SMC FORMULATION

The generalized optical theorem and a related property, the unitarity of the S matrix, are completely general properties that a scattering calculation must satisfy. Since the SMC formulation is derived from a combination of the projected Lippmann-Schwinger equation and the Schrödinger equation, it remains to be shown whether the generalized optical theorem holds in this formulation and also under what conditions the unitarity of the S matrix is satisfied. First we rewrite Eq. (10) with explicit energy dependence,

$$T_{mn}=\frac{\langle S_m(\mathcal{E})|V|\Psi_n^{(+)}(\mathcal{E})\rangle\langle\Psi_m^{(-)}(\mathcal{E})|V|S_n(\mathcal{E})\rangle}{\langle\Psi_m^{(-)}(\mathcal{E})|A^{(+)}(\mathcal{E})|\Psi_n^{(+)}(\mathcal{E})\rangle} . \tag{11}$$

Equation (11) corresponds to an on-the-energy-shell T matrix with

$$\mathcal{E}=E_n+\tfrac{1}{2}k_n^2=E_m+\tfrac{1}{2}k_m^2 . \tag{12}$$

We now generalize the on-the-energy-shell T matrix to off-the-energy shell. Let

$$\mathcal{E}_m=E_m+\tfrac{1}{2}k_m^2 , \tag{13a}$$

$$\mathcal{E}_n=E_n+\tfrac{1}{2}k_n^2 . \tag{13b}$$

Here $\mathcal{E}_m$ may not be equal to $\mathcal{E}_n$. Following the notation of Newton,[29] we define the off-the-energy-shell T matrix $T_{mn}^{(+)}$ as

$$T_{mn}^{(+)}=\frac{\langle S_m(\mathcal{E}_m)|V|\Psi_n^{(+)}(\mathcal{E}_n)\rangle\langle\Psi_m^{(-)}(\mathcal{E}_m)|V|S_n(\mathcal{E}_n)\rangle}{\langle\Psi_m^{(-)}(\mathcal{E}_m)|A^{(+)}(\mathcal{E}_n)|\Psi_n^{(+)}(\mathcal{E}_n)\rangle} . \tag{14}$$

The Hermitian conjugate of $T_{mn}^{(+)}$ is

$$T_{nm}^{(+)*}=\frac{\langle S_m(\mathcal{E}_m)|V|\Psi_n^{(+)}(\mathcal{E}_n)\rangle\langle\Psi_m^{(-)}(\mathcal{E}_m)|V|S_n(\mathcal{E}_n)\rangle}{\langle\Psi_m^{(-)}(\mathcal{E}_m)|A^{(-)}(\mathcal{E}_m)|\Psi_n^{(+)}(\mathcal{E}_n)\rangle} . \tag{15}$$

Here we have made use of the Hermitian property of the operators $PV+VP$ and $\hat{H}-(N+1/2)(P\hat{H}+\hat{H}P)$.

Taking the difference between $T^{(+)}_{mn}$ and $T^{(+)*}_{nm}$, we find after some minor regrouping of terms

$$T^{(+)}_{mn}-T^{(+)*}_{nm}=\frac{\langle S_m(\mathcal{E}_m)\mid V\mid\Psi^{(+)}_n(\mathcal{E}_n)\rangle\langle\Psi^{(-)}_m(\mathcal{E}_m)\mid V\mid S_n(\mathcal{E}_n)\rangle}{\langle\Psi^{(-)}_m(\mathcal{E}_m)\mid A^{(+)}(\mathcal{E}_n)\mid\Psi^{(+)}_n(\mathcal{E}_n)\rangle\langle\Psi^{(-)}_m(\mathcal{E}_m)\mid A^{(-)}(\mathcal{E}_m)\mid\Psi^{(+)}_n(\mathcal{E}_n)\rangle}$$

$$\times\{\langle\Psi^{(-)}_m(\mathcal{E}_m)\mid VG^{(+)}_P(\mathcal{E}_n)V-VG^{(-)}_P(\mathcal{E}_m)V\mid\Psi^{(+)}_n(\mathcal{E}_n)\rangle$$

$$+\langle\Psi^{(-)}_m(\mathcal{E}_m)\mid\tfrac{1}{2}[P\hat{H}(\mathcal{E}_n)+\hat{H}(\mathcal{E}_n)P-P\hat{H}(\mathcal{E}_m)-\hat{H}(\mathcal{E}_m)P]$$

$$+\frac{1}{N+1}[\hat{H}(\mathcal{E}_m)-\hat{H}(\mathcal{E}_n)]\mid\Psi^{(+)}_n(\mathcal{E}_n)\rangle\}\ . \tag{16}$$

Letting $\mathcal{E}_m\rightarrow\mathcal{E}_n$, we obtain the following relationship for the on-the-energy-shell T matrix:

$$T_{mn}-T^*_{nm}=\frac{1}{(2\pi)^3}\int d\epsilon_k\int d\hat{k}\sum_{l=1}^{M}\langle\Psi^{(-)}_m\mid V\mid\Phi_l\exp(i\mathbf{k}\cdot\mathbf{r}_{N+1})\rangle\langle\Phi_l\exp(i\mathbf{k}\cdot\mathbf{r}_{N+1}\mid V\mid\Psi^{(+)}_n\rangle$$

$$\times\left[\frac{1}{(\mathcal{E}-E_l)-\epsilon_k+i\delta}-\frac{1}{(\mathcal{E}-E_l)-\epsilon-i\delta}\right] \tag{17}$$

with $\epsilon_k=k^2/2$. The two principal-value integrals cancel each other. Only the residues contribute to Eq. (17). Letting $k_l^2/2=\mathcal{E}-E_l$, we find

$$T_{mn}-T^*_{nm}=-2\pi i\sum_{l=1}^{M}\int d\hat{k}_l\langle\Psi^{(-)}_m\mid V\mid S_l\rangle\langle S_l\mid V\mid\Psi^{(+)}_n\rangle\ . \tag{18}$$

Here $\hat{k}_l$ denotes the angular coordinates of $\mathbf{k}_l$. The right side of Eq. (18) is just $T_{ml}T^*_{nl}$ in the conventional T-matrix expression. Making use of Eq. (8) we can rewrite them in the fractional form

$$T_{mn}-T^*_{nm}=-2\pi i\sum_{l=1}^{M}\int d\hat{k}_l\frac{\langle\Psi^{(-)}_m\mid V\mid S_l\rangle\langle S_m\mid V\mid\Psi^{(+)}_l\rangle}{\langle\Psi^{(-)}_m\mid A^{(+)}\mid\Psi^{(+)}_l\rangle}\frac{\langle\Psi^{(-)}_l\mid V\mid S_n\rangle\langle S_l\mid V\mid\Psi^{(+)}_n\rangle}{\langle\Psi^{(-)}_l\mid A^{(-)}\mid\Psi^{(+)}_n\rangle}\ . \tag{19}$$

We now obtain the generalized optical theorem in the SMC formulation

$$T_{mn}-T^\dagger_{mn}=-2\pi i\sum_{l=1}^{M}\int d\hat{k}_l T_{ml}T^\dagger_{ln}\ . \tag{20}$$

Notice that Eq. (20) is satisfied as long as the residues of the k integral in Eq. (17) are evaluated correctly. It is independent of the principal-value contributions.

In the case when $\Psi^{(+)}_n$ is in the angular momentum representation instead of linear momentum representation, the generalized optical theorem can be obtained by expanding $\Psi^{(+)}_n$ in a Legendre series. The SMC expression for the T matrix becomes

$$T_{m\lambda_m\mu_m,n\lambda_n\mu_n}=\frac{\langle S_{m\lambda_m\mu_m}(\mathcal{E})\mid V\mid\Psi^{(+)}_{n\lambda_n\mu_n}(\mathcal{E})\rangle\langle\Psi^{(-)}_{m\lambda_m\mu_m}(\mathcal{E})\mid V\mid S_{n\lambda_n\mu_n}(\mathcal{E})\rangle}{\langle\Psi^{(-)}_{m\lambda_m\mu_m}(\mathcal{E})\mid A^{(+)}(\mathcal{E})\mid\Psi^{(+)}_{n\lambda_n\mu_n}(\mathcal{E})\rangle}\ , \tag{21}$$

where λ labels the angular momentum associated with the incoming (outgoing) electron and μ its projection on the z axis. After some straightforward manipulation, we find

$$T_{m\lambda_m\mu_m,n\lambda_n\mu_n}-T^\dagger_{m\lambda_m\mu_m,n\lambda_n\mu_n}=-2\pi i\sum_{l=1}^{M}\sum_{\lambda_l=0}^{\infty}\sum_{\mu_l=0}^{\infty}T_{m\lambda_m\mu_m,l\lambda_l\mu_l}T^\dagger_{l\lambda_l\mu_l,n\lambda_n\mu_n}\ . \tag{22}$$

This is the generalized optical theorem in the angular momentum wave representation.

To relate the generalized optical theorem with the unitarity of the S matrix, we use the relationship

$$S=1-2\pi iT\ . \tag{23}$$

The unitarity of the S matrix requires that

$$S(\mathcal{E})S^\dagger(\mathcal{E})=S^\dagger(\mathcal{E})S(\mathcal{E})=1\ . \tag{24}$$

Since

$$S(\mathcal{E})S^\dagger(\mathcal{E})=[1-2\pi iT(\mathcal{E})][1+2\pi iT^\dagger(\mathcal{E})]$$

$$=1-2\pi i[T(\mathcal{E})-T^\dagger(\mathcal{E})]+4\pi^2T(\mathcal{E})T^\dagger(\mathcal{E})\ , \tag{25}$$

the unitarity of the S matrix requires the relationship

$$T(\mathcal{E})-T^\dagger(\mathcal{E})=-2\pi iT(\mathcal{E})T^\dagger(\mathcal{E}) \tag{26}$$

to be satisfied. In the angular momentum representation,

with the number of open channels limited to M, we have

$$T_{m\lambda_m\mu_m,n\lambda_n\mu_n}-T^{\dagger}_{m\lambda_m\mu_m,n\lambda_n\mu_n} = -2\pi i\sum_{l=1}^{M}\sum_{\lambda_l=0}^{\infty}\sum_{\mu_l=0}^{\infty}T_{m\lambda_m\mu_m,l\lambda_l\mu_l}T^{\dagger}_{l\lambda_l\mu_l,n\lambda_n\mu_n} . \quad (27)$$

Equation (27) is identical to Eq. (22). Based on the discussions immediately following Sec. I, we conclude that Eq. (27), and hence the unitarity of the S matrix, will be satisfied as long as the residue of the $VG_P^{(+)}V$ term is calculated correctly and a sufficient number of partial waves are used in the expansion.

While the preceding derivation assumes that $\Psi_n^{(+)}$ is an exact solution, it can be shown in a straightforward manner that, even if $\Psi_n^{(+)}$ is the solution to an approximate $A^{(+)}$, the unitarity condition still holds as long as the residue of the $VG_P^{(+)}V$ is evaluated correctly. Based on this property, we introduced a procedure in which an insertionlike quadrature is used to represent $G_P^{(+)}$ in evaluating its principal-value contribution, but the residue of the $VG_P^{(+)}V$ term is calculated analytically,

$$-\pi i\sum_{l=1}^{M}\int d\hat{k}_l\langle\Psi_m^{(-)}\mid V\mid S_l\rangle\langle S_l\mid V\mid\Psi_n^{(+)}\rangle . \quad (28)$$

The integration over $\hat{k}_l$ is carried out numerically. Nearly perfect unitarity (limited only by the number of angular momentum waves) is obtained. This will be discussed in more detail in Sec. IV.

IV. COMPUTATIONAL PROCEDURES

In the present calculation, we consider only e-N_2 elastic scattering below the first electronically inelastic threshold. The total wave function $\Psi_0^{(+)}$ is expanded in a basis of $(N+1)$-particle Slater determinants, ψ_i,

$$T_{00}=\sum_{i,j}\langle S_0\mid V\mid\psi_i\rangle A^{-1}_{ij}\langle\psi_j\mid V\mid S_0\rangle . \quad (29)$$

The Slater determinants are constructed from an orthogonal set of molecular orbitals which are in turn expanded in a set of Cartesian Gaussian functions. With this choice of basis, all the matrix elements appearing in Eq. (29), except for those of $VG_P^{(+)}V$, can be evaluated for molecules of arbitrary geometry.[22] Furthermore, the $VG_P^{(+)}V$ matrix elements can be obtained in closed form using the following procedure. The principal-value contribution to the $VG_P^{(+)}V$ matrix element is obtained by inserting a large set of Cartesian Gaussian functions around $G_P^{(+)}$, whereas the contribution from the poles of $G_P^{(+)}$ is evaluated analytically. As discussed in Sec. III, this procedure results in an S matrix which is very nearly unitary without resorting to a very large quadrature basis.

A. Gaussian basis set for $\Psi_0^{(+)}$

Two different Gaussian basis sets have been used in the representation of $\Psi_0^{(+)}$. In both cases we started with the $9s5p2d/5s3p2d$ basis set used by Langhoff *et al.*[30] in their calculation of the static polarizability of N_2. Their values for $\alpha_\parallel$ calculated with an SCF and CI wave function at the experimental R_e are 14.908 and 14.868 a.u., respectively, compared with the experimental values of 15.05 (Ref. 31) and 14.76 (Ref. 32). The SCF and CI values for $\alpha_\perp$ are 9.514 and 10.196 a.u., versus experimental values of 10.35 (Ref. 31) and 10.25 (Ref. 32). We uncontracted this basis set and added diffuse functions $2s$, $3p$, and $1d$ to obtain a $11s8p3d$ set. The need for diffuse s and p functions was demonstrated in a static-exchange calculation with an s,p basis set. It was found that the inclusion of diffuse functions changed both the position and width of the resonance. In Gaussian set A, we dropped the d_{x^2},d_{y^2}, and the two most diffuse d_{xy} because the $d\delta$ functions are unimportant for radial correlation, the most important correlation effect in this channel. Using the SCF wave function calculated with this basis set, the quadrupole moment of N_2 is determined at the SCF R_e to be $-0.936ea_0^2$ a.u., compared with an experimental value[33] of $-1.04\pm0.07ea_0^2$. In Gaussian set B we dropped the most diffuse d_{x^2}, d_{y^2}, and d_{z^2} functions. The quadrupole moment determined with this basis is $-0.940ea_0^2$. Both basis sets are tabulated in Table I.

B. Insertion basis set for $G_p^{(+)}$

While the choice of the Gaussian basis set, molecular orbitals, and Slater determinants in the representation of $\Psi_0^{(+)}$ can be partly based on physical considerations such as calculations of other properties, the separable L^2 representation of $G_P^{(+)}$ is of a more mathematical nature. The quality of the solution of Eq. (8) depends on the completeness of this insertion basis and care must be exercised in its choice. In our earlier application of the SMC method,[21,34] all contributions to the $VG_P^{(+)}V$ matrix element were determined with such a separable L^2 representation of the Green's function using Gaussian functions (α insertion), and the unitarity of the calculated S matrix was used as the criterion for the completeness of the insertion basis. We have since adopted the practice of calculating the contribution from the poles of $G_P^{(+)}$ analytically and used the insertion basis only for the principal-value contri-

TABLE I. Gaussian basis set used in the representation of $\Psi_0^{(+)}$. All basis functions are centered at the nuclei.

Type	Exponent
Gaussian set A	
s	5909.0, 887.5, 204.7, 59.84, 20.0, 7.193, 2.686, 0.7, 0.2133, 0.07, 0.03
p_x,p_y,p_z	26.79, 5.956, 1.707, 0.5314, 0.1654,
d_{zz},d_{xz},d_{yz}	0.06, 0.02, 0.01, 0.95, 0.2639, 0.06
d_{xy}	0.95
Gaussian set B	
s	5909.0, 887.5, 204.7, 59.84, 20.0, 7.193, 2.686, 0.7, 0.2133, 0.07, 0.03
p_x,p_y,p_z	26.79, 5.956, 1.707, 0.5134, 0.1654,
d_{zz},d_{xx},d_{yy}	0.06, 0.02, 0.01, 0.95, 0.2639
d_{xz},d_{yz}	0.95, 0.2639, 0.06
d_{xy}	0.95, 0.2639, 0.06

bution (k insertion), resulting in an S matrix which is very close to unitarity. However, we reverted to α insertion in testing the insertion basis and depended on the unitarity of the S matrix as a guide, even though our final results were calculated using the k-insertion technique. This practice was based on the rationale that the principal-value contributions to $G_P^{(+)}$ are large and rapidly varying near its poles. Thus a good representation of the residues, as indicated by the unitarity, also implies a good representation of the principal value.

Our insertion basis always includes the original Gaussian basis set used for $\Psi_0^{(+)}$ because all the necessary integrals have already been calculated. Table II presents four sets of additional d_{xz} functions used in the $^2\Pi_{gx}$ channel calculation. Notice that none of the insertion basis contains very diffuse functions. This is somewhat surprising because normally such functions are expected to be important in a separable L^2 representation of $G_P^{(+)}$. Our original trial basis did include very diffuse d_{xz} functions but they were eliminated based on the unitarity criterion discussed above. This result reflects the quasi-bound-state character of the $^2\Pi_g$ channel and may not be generally applicable. We also found results near the resonance to be particularly sensitive to the choice of insertion basis. Figure 1 presents the eigenphase sum δ_{sum} as a function of incident electron energy at the target internuclear distance, $R=1.9$ a.u., calculated with the k-insertion technique using the insertion basis I and II. Separable calculations using only α insertion showed that basis I failed the unitarity condition completely at 0.25–0.27 Ry, but at other energies the unitarity condition was rather well satisfied. For basis II the largest deviation from unitarity was 9%. It is seen that the two curves are in good agreement except in the region where unitarity fails in the α insertion using basis I. It should be remembered that the data used in the figure were actually calculated using k insertion and perfect unitarity is obtained at all energies, even for basis I. We consider that the results in Fig. 1 justify our use of the α-insertion technique and unitarity condition as a guide in the choice of an insertion basis. Figure 1 also demonstrates the importance of a good insertion basis in a Schwinger-type calculation since an erroneous width would be deduced if set I were used.

Since the resonance energy is R dependent, the fact that the insertion basis is sensitive to the position of the resonance means that different insertion basis must be used for different R's. Insertion basis I was used in the calculation at $R=2.3$, 2.2, and 2.068 a.u. and the nonresonant region at $R=1.9$ a.u. Basis II was used at 2.1 a.u. as well as the resonant region of 1.9 a.u. Basis sets III and IV were used at 1.8 and 1.7 a.u. respectively. It was found that Gaussians with large exponents are needed as R decreases and the resonance position moves to higher energy. In general, the lower the resonance energy, the easier it is to satisfy the unitarity condition. For example, at 2.2 a.u. the largest deviation from unitarity found in an α-insertion calculation is 4%, whereas at 1.7 a.u. the deviation is 25%, even with a large set of insertion functions.

C. Choice of molecular orbitals and closed-channel configurations

In our calculation, a SCF wave function is used to represent the target in the asymptotic region of the configuration space. In the static-exchange approximation, the $(N+1)$-particle wave function is expanded in terms of the following set of Slater determinants:

$$\Psi_0^{(+)}=\sum_k c_k \mathcal{A}(\phi_1\phi_2\cdots\phi_n\phi_k)\ , \tag{30}$$

where $\mathcal{A}$ is the antisymmetrization operator, $\phi_1,\phi_2,\ldots,\phi_n$ are target SCF orbitals, and ϕ_k is an orbital generated from the Gaussian set for $\Psi_0^{(+)}$ and orthogonalized to the target orbitals. Since the full set of ϕ_k is used on the right-hand side of Eq. (30), the result is invariant with respect to a unitary transformation of the ϕ's. However, in a correlation (polarization) calculation, $\Psi_0^{(+)}$ is represented by a polarization configuration-interaction (POLCI) wave function,[35]

$$\Psi_0^{(+)}=\sum_k c_k \mathcal{A}(\phi_1\phi_2\cdots\phi_n\phi_k) + \sum_{i,j,k} c_{ij,k} a_j a_i^\dagger \mathcal{A}(\phi_1\phi_2\cdots\phi_n\phi_k)\ , \tag{31}$$

TABLE II. Gaussian basis set used in the representation of $G_p^{(+)}$.

Basis set	Exponent of d_{xz} functions at midpoint
Set I: Basis set from Table I plus 10 d_{xz} functions at midpoint	240, 120, 60, 30, 15, 8, 4, 2, 1, 0.25
Set II: Basis set from Table I plus 15 d_{xz} functions at midpoint	4800, 2400, 1200, 600, 480, 240, 120, 60, 30, 15, 8, 4, 2, 1, 0.25
Set III: Basis set from Table I plus 22 d_{xz} functions at midpoint	9600, 7200, 4800, 2400, 1200, 800, 600, 400, 300, 200, 120, 80, 60, 40, 24, 16, 8, 4, 2, 1, 0.5, 0.25
Set IV: Basis set from Table I plus 25 d_{xz} functions at midpoint	32 400, 21 800, 17 200, 9600, 7200, 4800, 2400, 1200, 800, 600 400, 300, 200, 120, 80, 60, 40, 24, 16, 8, 4, 2, 1, 0.5, 0.25

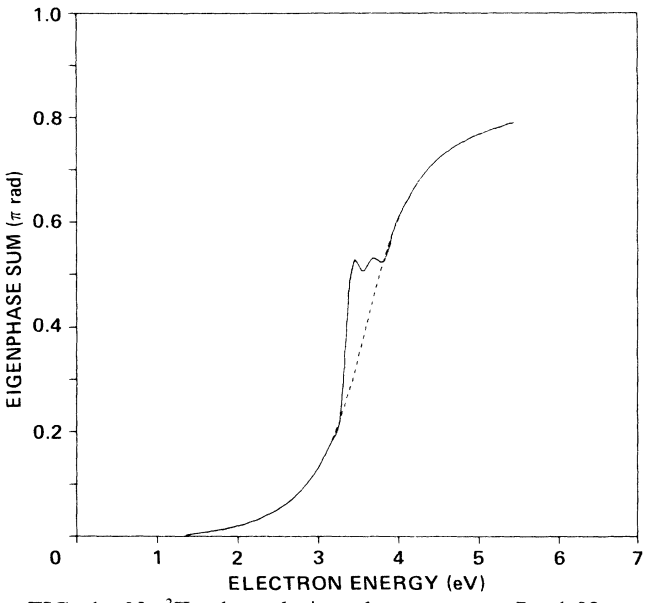

FIG. 1. N_2 $^2\Pi_g$-channel eigenphase sums at $R=1.90$ a.u. calculated using insertion basis I (——) and insertion basis II (— — —).

where the operator $a_i^\dagger$ annihilates an electron occupying a target orbital ϕ_i, a_j creates an electron in orbital ϕ_j, and $c_{ij,k}$ is the coefficient associated with this closed-channel configuration. The closed-channel configurations describe the mutual distortion of the incoming electron and the target. Our present computer codes are limited in the total number of Slater determinants used in $\Psi_0^{(+)}$. Since this is far from the size of the full set of all possible closed-channel configurations, a judicious choice of the orbital basis and closed-channel configurations must be made to achieve reliable results. While our code is being extended, we feel that the procedure used in the N_2 calculation is physically meaningful and a description is given here.

Two different orbital sets were tried: virtual orbitals from the target SCF calculation with the π_g orbitals replaced by the corresponding set obtained from an improved virtual orbital[36] calculation on the $^2\Pi_g$ state of N_2^-, and the set of natural orbitals obtained from a standard bound-state POLCI (Ref. 35) calculation for N_2^-. Within the limitation of the present SMC code, essentially no correlation effects could be obtained using the first set. This is due to the inadequacy of the virtual orbitals in describing the distortion of the target and the slow convergence of the closed-channel expansion in this orbital basis. On the other hand, a bound state POLCI calculation (including all possible configurations) can be used efficiently in describing the relaxation of the target in the presence of an extra electron. The use of a bound-state code to determine the N_2^- wave function, without imposing any stabilization constraint or the correct boundary condition, actually results in a N_2^- wave function which is a mixture of continuum and bound states. Nevertheless, the natural orbitals from such a calculation, ordered according to their occupation in the density matrix, enables us to truncate the set of orbitals used for the closed-channel configurations. While we cannot carry out the full expansion in Eq. (31) to establish convergence, we find that cutting back the orbitals used in the second expansion in Eq. (31) by half results in a 3% change in the calculated cross section near resonance, giving us confidence that the truncation of the orbitals based on the natural orbitals is indeed valid. It should be noted that the full set of orbitals are used in the first sum in Eq. (31) (static-exchange terms) and orbital truncation is only done in the second sum (correlation terms). Table III presents the truncated orbital basis used in the correlation calculations.

The closed-channel configurations describe the correlation effects between the scattered electron and the bound electrons. The pair functions used to describe this correlation can be divided into two types: radial correlation (or in-out correlation) where each electron is promoted (or demoted) into an orbital of the same symmetry, and angular correlation where each electron is promoted to an orbital of different symmetry. Schneider and Collins[15] first discussed the effect of such terms in their study of e-N_2 scattering using the linear-algebraic-optical-potential method. They identified the radial correlation as a short-range correlation. The angular correlation, with electron promotion limited to dipole-allowed configurations, was identified as a long-range correlation since it reduces to the r^{-4} potential at large r. Nevertheless, the angular correlation terms include a short-range component also. The effects of these correlation terms were studied in our determination of important closed-channel configurations. We started by studying the effect of correlating individual pairs, e.g., the $3\sigma_g$ electron with the continuum electron, with all possible radial and angular correlation terms included. We found virtually no effect in correlating the $1\sigma_g$, $1\sigma_u$, and $2\sigma_g$ electrons and a small effect in correlating the $2\sigma_u$. The most important contribution comes from correlating

TABLE III. Closed-channel configurations used for the $^2\Pi_{gx}$ channel.

ϕ_i	ϕ_j	ϕ_k
Set I		
$3\sigma_g$	4, 5, 6, $7\sigma_g$	1, 2, 3, 4, $5\pi_{gx}$
$1\pi_{ux}$	2, 3, 4, $5\pi_{ux}$	1, 2, 3, 4, $5\pi_{gx}$
$1\pi_{uy}$	2, 3, 4, $5\pi_{uy}$	1, 2, 3, 4, $5\pi_{gx}$
Set II		
$3\sigma_g$	4, 5, 7, 8, $9\sigma_g$	1, 2, 3, 4, $5\pi_{gx}$
$1\pi_{ux}$	2, 3, 4, 5, $6\pi_{ux}$	1, 2, 3, 4, $5\pi_{gx}$
$1\pi_{uy}$	2, 3, 4, 5, $6\pi_{uy}$	1, 2, 3, 4, $5\pi_{gx}$
$2\sigma_u$	3, 4, 5, $6\sigma_u$	1, 2, 3, $4\pi_{gx}$
$2\sigma_g$	4, 5, 7, $8\sigma_g$	1, 2, 3, $4\pi_{gx}$
$3\sigma_g$	3, $4\sigma_u$	2, 3, $4\pi_{ux}$
$3\sigma_g$	2, $3\pi_{ux}$	3, 4, $5\sigma_u$
$3\sigma_g$	2, $3\pi_{uy}$	1, 2, $3\delta_{uxy}$
$1\pi_{ux}$	4,$5\sigma_g$	3, 4, $5\sigma_u$
$1\pi_{ux}$	1, $2\pi_{gx}$	2, 3, $4\pi_{ux}$
$1\pi_{ux}$	1, $2\delta_{gxy}$	1, 2, $3\delta_{uxy}$
$1\pi_{uy}$	4, $5\sigma_g$	1, 2, $3\delta_{uxy}$
$1\pi_{uy}$	1, $2\pi_{gy}$	2, 3, $4\pi_{ux}$
$1\pi_{uy}$	1, $2\delta_{gxy}$	3, 4, $5\sigma_u$

the six outermost electrons in $3\sigma_g$, $1\pi_{ux}$, and $1\pi_{uy}$ orbitals. Based on our results on the individual pair correlations, we chose two sets of closed-channel configurations. In set I, we included only radial correlation terms for the six valence electrons. In set II, we included radial and angular correlations for the six valence electrons as well as radial correlation terms for the $2\sigma_g$ and $2\sigma_u$ electrons. In the terminology of Schneider and Collins,[15] set I corresponds to a 13-reference calculation and set II is a 42-reference calculation. Also, in all the calculations reported below, Gaussian basis set *A* was used together with closed-channel configuration set I and Gaussian basis set *B* was used with closed-channel configuration set II.

V. RESULTS AND DISCUSSIONS

Figure 2 compares the eigenphase sums δ_{sum}, at $R=2.068$ a.u. using the two sets of closed-channel configurations. Also presented are the eigenphase sums from Hazi's Stieltjes imaging calculation[5,6] and the many-body optical potential calculation by Berman and Domcke.[11] We find good agreement between our set I results and both previous calculation. This is not surprising since the calculations in Refs. 5 and 11 include only radial correlation effects. Notice that the present calculation includes both resonant and nonresonant contributions to δ_{sum}. There is no direct means to separate the two contributions in the SMC formulation. The δ_{sum} of Berman and Domcke also includes both resonant and nonresonant terms even though they are calculated separately in the many-body optical potential formulation. On the other hand, the Stieltjes calculation of Hazi[6] determines only the resonant contribution to δ_{sum}. Since the nonresonant contribution for this channel in N_2 is very small at the energies considered here,[11] a comparison between our result and Hazi's is still valid. Nevertheless, some of the discrepancies between the two results for far off resonance may be due to the nonresonant contributions.

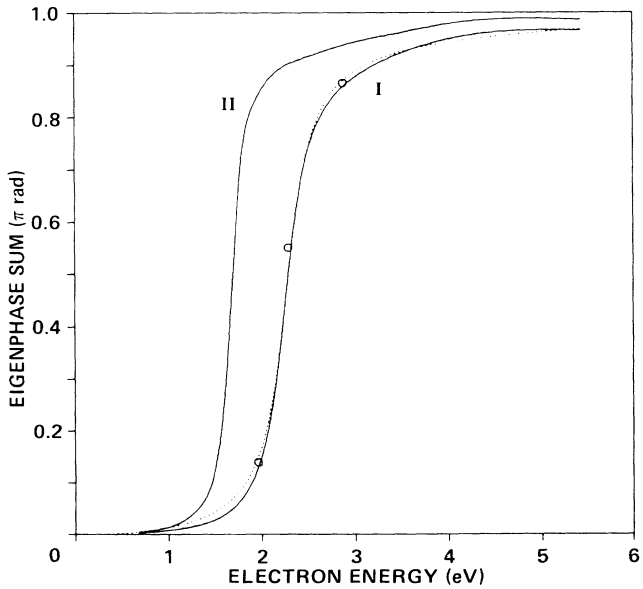

FIG. 2. N_2 $^2\Pi_g$-channel eigenphase sums at $R=2.068$ a.u. calculated using closed-shell configurations sets I and II (——), the Stieltjes calculations by Hazi from Ref. 6 (· · ·), and the many-body optical potential calculation by Berman and Domcke from Ref. 11 (○).

Comparing the results using two different sets of closed-channel configurations, we found significant differences between the results calculated using closed-channel configurations I and II. The resonance energy deduced from set I is 2.29 eV and from set II, 1.70 eV. This result is similar to those obtained by Schneider and Collins who deduced a resonance energy of 2.07 eV with radial correlation alone and 1.66 eV with both radial and angular correlations. Also, the elastic[25] and vibrational excitation[26] cross sections calculated with set I are in good agreement with experiment, whereas a set-II calculation shifts the resonance position to a much lower energy than that observed experimentally. The width from set II is also too narrow.

It may be worthwhile to comment on possible reasons for the discrepancy between the two sets of results. It is well known that angular correlation is dominant in N_2.[37] Due to antisymmetrization, correlation in the $(N+1)$-electron system automatically implies certain correlations in the target—the recorrelation problem. If angular correlation is introduced in the scattering system, consistency requires an adequately correlated description of the target. This would result in lowering the target energy and gives rise to an increase in the calculated resonance energy, bringing the result to a better agreement with experiment. Indeed, a recent calculation by Weatherford *et al.*[38] using a correlated target wave function together with a semiempirical polarization potential suggests this to be the case. Thus, we conclude that the treatment of correlation in set II is *not* incorrect. Instead, our result indicates that a more sophisticated treatment of electron-target correlation simultaneously demands a more sophisticated treatment of the target itself.

Figure 3 compares the $^2\Pi_g$-channel cross sections at 2.068 a.u. with the results of Morrison and Collins[39] and Gibson *et al.*[40] The calculations by Morrison and Collins, using the free-electron gas exchange potential and a heuristic polarization potential, are in reasonable agreement with our set-I results. Gibson *et al.* employed an *ab initio* polarization potential determined using a variational method. Their results are in good agreement with our set-I calculations but differ significantly from our set-II cross sections. The agreement with the former belies the different physical approximations used in these two calculations. While our set-I calculations included only radial correlation, the polarization potential of Gibson *et al.* was calculated with the nonpenetrating approximation.[41] In that procedure the monopole term in the Coulomb potential, primarily responsible for radial correlations, is omitted. It is likely that the differences between their results and our set-II calculations are also due to the approximate treatment of the short-range correlations in their polarization potential. Further insight into the nature of this type of polarization potential can be obtained when future calculations for systems other than H_2 and N_2 are compared with *ab initio* treatments.

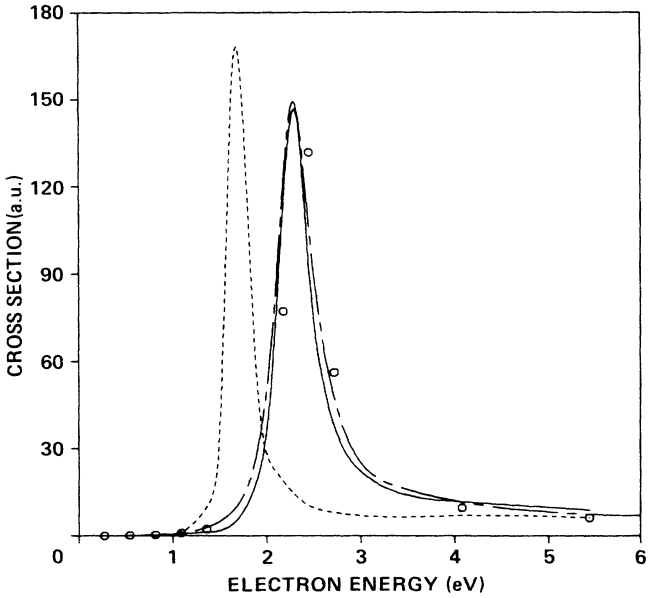

FIG. 3. N_2 $^2\Pi_g$-channel cross sections at $R = 2.068$ a.u. calculated using closed-shell configurations set I (——), set II (— — —), by Gibson, Saha, and Morrison, Ref. 40 (—·—·—), and by Morrison and Collins, Ref. 39 (○).

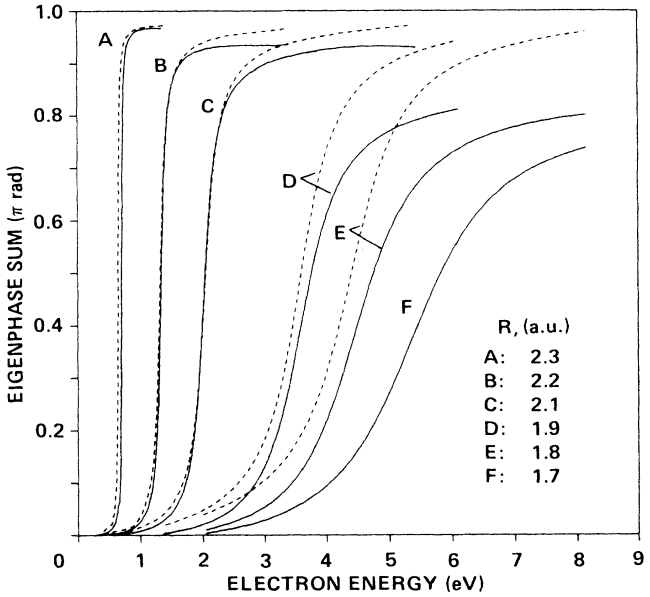

FIG. 4. N_2 $^2\Pi_g$-channel eigenphase sums calculated at $R = 1.7$ to 2.3 a.u. using closed-shell configuration set I (——) and the Stieltjes calculation by Hazi from Ref. 6 (— — —).

Figure 4 plots the eigenphase sums at $R = 1.7$, 1.8, 1.9, 2.1, 2.2, and 2.3 a.u. calculated using closed-shell configuration set I. For comparison purposes, we also present the δ_{sum} from the Stieltjes imaging calculation of Hazi[6] at $R = 1.8$–2.3 a.u. Hazi's calculations were carried out at a different set of R values and the data presented in Fig. 4 were deduced from interpolated values using a fitted formula.[42] At $R \geq 2.1$ a.u., agreement between the two sets of calculations is good except at the high-energy end of the curves. We believe this discrepancy is due to the nonresonant contribution to δ_{sum}, which is not included in Hazi's calculation. For $R < 1.9$ a.u. the resonance position moves to above 3 eV and we find significant discrepancies between the two sets of calculations, especially at the high-energy end. While part of this deviation may be due to the differences between the two computational methods, the correlation between the resonance position and percen-

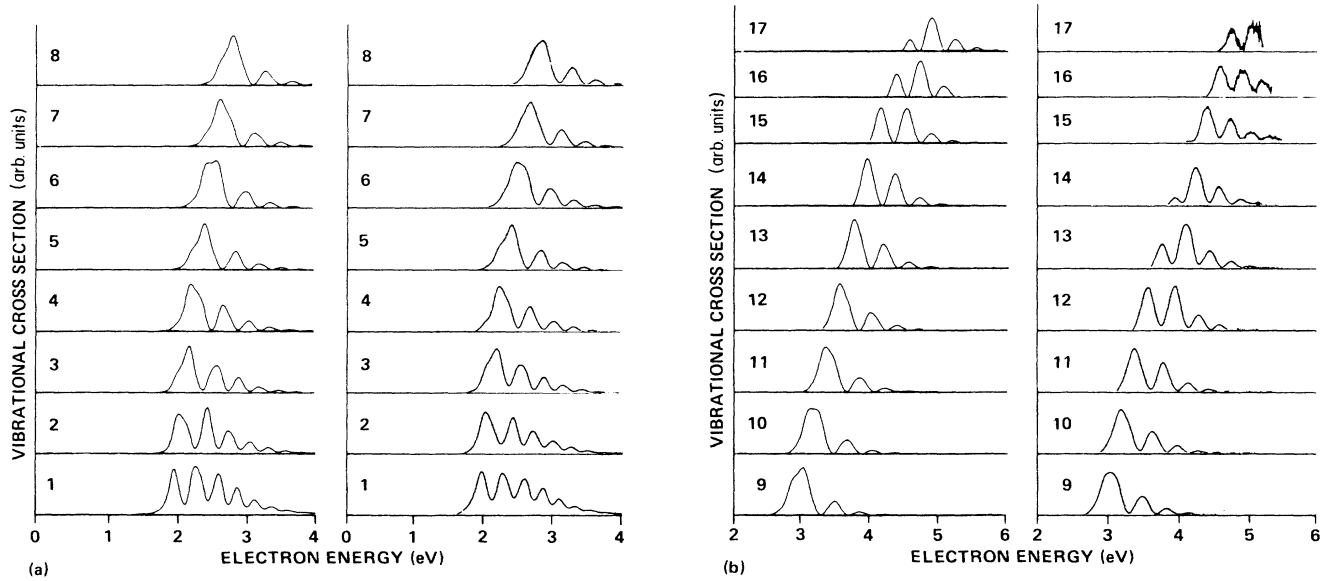

FIG. 5. (a) (b) Vibrational excitations for the $v''=0 \rightarrow v'$ transitions in e-N_2 scattering. Spectra on the left are from present calculation, and on the right, the experimental results of Allan (Ref. 44).

TABLE IV. Positions and magnitudes of the maxima in the cross sections. Cross sections are in cm^2 with powers of ten in square brackets.

Transition	Energy (eV)			Cross section (cm^2)		
	Present	Allan[a]	Morgan[b]	Present	Allan[a]	Morgan[b]
0→1	1.96[c]	1.95	2.12	5.75[−16]	5.6[−16]	6.94[−16]
0→2	2.00[c]	2.00	2.32	3.30[−16]	3.7[−16]	3.39[−16]
0→3	2.18	2.15	2.40	2.90[−16]	3.1[−16]	3.09[−16]
0→4	2.22	2.22	2.62	1.79[−16]	2.1[−16]	1.39[−16]
0→5	2.42	2.39	2.68	1.23[−16]	1.3[−16]	8.9[−17]
0→6	2.48[c]	2.48	2.93	5.24[−17]	7.1[−17]	3.7[−17]
0→7	2.66	2.64	2.99	3.04[−17]	3.8[−17]	1.3[−17]
0→8	2.87	2.82	3.25	1.31[−17]	1.6[−17]	5.0[−18]
0→9	3.06	2.95	3.50	4.57[−18]	6.1[−18]	1.5[−18]
0→10	3.16	3.09	3.75	1.44[−18]	2.2[−18]	3.5[−19]
0→11	3.35	3.30	3.97	4.67[−19]	6.3[−19]	6.8[−20]
0→12	3.55	3.87	4.15	1.31[−19]	1.4[−19]	1.2[−20]
0→13	3.75	4.02	4.85	3.23[−20]	4.5[−20]	1.9[−21]
0→14	3.96	4.16	5.08	7.06[−21]	1.3[−20]	4.7[−22]
0→15	4.16	4.32	5.30	1.37[−21]	3.6[−21]	9.7[−23]
0→16	4.71	4.49	5.52	3.62[−22]	9.1[−22]	1.8[−23]
0→17	4.88	4.66	5.72	0.96[−22]	2.4[−22]	2.7[−24]

[a]Reference 44.
[b]Reference 9.
[c]First maximum. Calculated second maximum is slightly higher.

tage deviation leads us to believe that most of the difference is again due to nonresonant contributions. From this result, it is obvious that the resonant and nonresonant contributions must be separated in order to determine the resonance energy and width correctly.

We use the results of these calculations to obtain resonant vibrational excitation cross sections. The required width and shift functions were deduced from the K matrix of the $l=2$, $m=1$ partial-wave channel. Nuclear dynamics calculations were carried out based on the Feshbach projection operator formulation of Berman *et al.*[42] The potential energy curve for the neutral molecule is taken to be the Rydberg-Klein-Rees (RKR) curve[43] and for the negative ion we use the semiempirical curve of Berman *et al.*[42] Further details of these calculations, as well as vibrational excitation cross sections for initial states $v''=0-12$ and $\Delta v=1-5$, have been presented elsewhere.[26] Figures 5(a) and 5(b) compare the present result for excitation from $v''=0$ to $v'=1-17$ with the experimental spectrum of Allan.[44] The overall agreement for levels up to $v'=11$ is good, including the substructure observed in the form of shoulders. For levels $v'=12$ and higher, the observed peak structure is not correctly reproduced by the present results. These differences are most probably due to the inadequacies of the potential energy curves assumed for the negative ion. Note that the calculated peak structures for $v'=15$, 16, and 17 are actually very similar (with an energy shift) to those observed experimentally for $v'=12$, 13, and 14. We summarize the results of these figures by tabulating the position of the maximum peaks and their cross sections in Table IV. The experimental data are normalized to the absolute cross section of Jung *et al.*[45] The relative cross sections are reported to have an uncertainty of ±20%.[44] Also presented in Table IV are the calculated results of Morgan[9] using the R-matrix method. On the average, our results agree better with experiment than those of Morgan.[9]

VI. CONCLUSIONS

In the present calculation electron-target correlation is treated on the same level of sophistication as in bound-state POLCI calculations. Our treatment of radial and angular correlations is applicable not only to the study of a shape resonance, but to nonresonant scattering as well (see the following paper). We believe this approach will be useful in other systems. Studies on e-CO and e-CH_4 are already under way.

The differential correlation effect in N_2 and N_2^-, invoked to explain the unusual behavior observed when angular correlations are incorporated into the calculation, should be studied further. Such studies are planned after our computer codes are modified to include correlated target systems.

ACKNOWLEDGMENTS

The research of W.M.H. is supported by NASA–Ames Cooperative Agreements No. NCC 2-147. The research at the California Institute of Technology is supported by NASA–Ames Cooperative Agreements No. NCC 2-319, the National Science Foundation, Grant No. PHY-8604242, and by the Innovative Science and Technology Program of the Strategic Defense Initiative Organization under Contract No. DAAL03-86-K-0140. One of us (M.A.P.L.) acknowledges the financial support from the Fundação de Amparo á Pesquisa do Estado de São Paulo (FAPESP), São Paulo, Brazil.

*Mailing address; NASA Ames Research Center, Mail Stop 230-3, Moffett Field, CA 94035.
†Present address: Department of Physics, Texas Tech University, Lubbock, TX 79409.
‡Present address: Instituto de Estudos Avançados, 12200 São José dos Campos, São Paulo, Brazil.

[1]G. J. Schulz, Rev. Mod. Phys. **45**, 423 (1973).
[2]S. Trajmar, D. F. Register, and A. Chutjian, Phys. Rep. **97**, 219 (1983).
[3]N. F. Lane, Rev. Mod. Phys. **52**, 29 (1980).
[4]B. I. Schneider, M. Le Dourneuf, and Vo Ky Lan, Phys. Rev. Lett. **43**, 1926 (1979).
[5]A. U. Hazi, T. N. Rescigno, and M. Kurilla, Phys. Rev. A **23**, 1089 (1981).
[6]A. U. Hazi, in *Electron-Atom and Electron-Molecule Collisions,* edited by J. Hinze (Plenum, New York, 1983), p. 103.
[7]P. G. Burke, C. J. Noble, and S. Salvini, J. Phys. B **16**, L113 (1983).
[8]M. Le Dourneuf, V. K. Lan, and B. I. Schneider, in *Electron-Atom and Electron-Molecule Collisions,* edited by J. Hinze (Plenum, New York, 1983), p. 135.
[9]L. A. Morgan, J. Phys. B **19**, L439 (1986).
[10]L. A. Collins, W. D. Robb, and M. A. Morrison, Phys. Rev. A **21**, 488 (1980).
[11]M. Berman and W. Domcke, Phys. Rev. A **29**, 2485 (1984).
[12]K. Onda and A. Temkin, Phys. Rev. A **28**, 621 (1983).
[13]C. A. Weatherford, K. Onda, and A. Temkin, Phys. Rev. A **31**, 3620 (1985).
[14]B. I. Schneider and L. A. Collins, Phys. Rev. A **27**, 2847 (1983).
[15]B. I. Schneider and L. A. Collins, Phys. Rev. A **30**, 95 (1984).
[16]T. N. Rescigno, A. E. Orel, and C. W. McCurdy, J. Chem. Phys. **73**, 6347 (1980).
[17]B. Nestmann and S. D. Peyerimhoff, J. Phys. B **18**, 615 (1985).
[18]B. Nestmann and S. D. Peyerimhoff, J. Phys. B **18**, 4309 (1985).
[19]K. Takatsuka and V. McKoy, Phys. Rev. A **24**, 1267 (1981).
[20]K. Takatsuka and V. McKoy, Phys. Rev. A **30**, 2473 (1984).
[21]T. L. Gibson, M. A. P. Lima, K. Takatsuka, and V. McKoy, Phys. Rev. A **30**, 3005 (1984).
[22]M. A. P. Lima, T. L. Gibson, W. M. Huo, and V. McKoy, Phys. Rev. A **32**, 2696 (1985).
[23]L. M. Brescansin, M. A. P. Lima, T. L. Gibson, V. McKoy, and W. M. Huo, J. Chem. Phys. **85**, 1854 (1986).
[24]M. A. P. Lima, T. L. Gibson, W. M. Huo, and V. McKoy, J. Phys. B **18**, L865 (1985).
[25]W. M. Huo, M. A. P. Lima, T. L. Gibson, and V. McKoy, following paper, Phys. Rev. A **36**, 1642 (1987). This paper will be referred to as II.
[26]W. M. Huo, V. McKoy, M. A. P. Lima, and T. L. Gibson, in *Thermophysical Aspects of Re-Entry Flows,* Vol. 103 of *Progress in Astronautics and Aeronautics,* edited by J. N. Moss and C. D. Scott (American Institute of Aeronautics and Astronautics, New York, 1986), p. 152.
[27]H. Feshbach, Ann. Phys. (N.Y.) **19**, 287 (1962).
[28]We have used a slightly different convention from previous work (Refs. 18–25) and incorporated the normalization factor of the plane wave in the expression of S_n. This convention is chosen for the convenience in the derivation of the optical theorem in Sec. III.
[29]R. G. Newton, *Scattering Theory of Waves and Particles* (McGraw-Hill, New York, 1966).
[30]S. R. Langhoff, C. W. Bauschlicher, Jr., and D. P. Chong, J. Chem. Phys. **78**, 5287 (1983).
[31]N. J. Bridge and A. D. Buckingham, Proc. R. Soc. London, Ser. A **295**, 334 (1966).
[32]G. R. Alms, A. W. Burham, and W. H. Flygare, J. Chem. Phys. **63**, 3321 (1975).
[33]A. D. Buckingham, R. L. Dish, and D. A. Dunmur, J. Chem. Soc. **90**, 3104 (1968).
[34]M. A. P. Lima, T. L. Gibson, K. Takatsuka, and V. McKoy, Phys. Rev. A **30**, 1741 (1984).
[35]P. J. Hay and T. H. Dunning, Jr., J. Chem. Phys. **64**, 5077 (1976).
[36]W. J. Hunt and W. A. Goddard III, Chem. Phys. Lett. **24**, 464 (1974).
[37]G. C. Lie and E. Clementi, J. Chem. Phys. **60**, 1288 (1974).
[38]C. A. Weatherford, F. B. Brown, and A. Temkin, Phys. Rev. A **35**, 4561 (1987).
[39]M. A. Morrison and L. A. Collins, Phys. Rev. A **17**, 918 (1978).
[40]T. L. Gibson, B. C. Saha, and M. A. Morrison, Phys. Rev. A (to be published).
[41]A. Temkin, Phys. Rev. **107**, 1004 (1957); A. Temkin, and J. C. Lamkin, *ibid.* **121**, 788 (1961).
[42]M. Berman, H. Estrada, L. S. Cederbaum, and W. Domcke, Phys. Rev. A **28**, 1363 (1983).
[43]A. Lofthus and P. H. Krupenie, J. Phys. Chem. Ref. Data **6**, 113 (1977).
[44]M. Allan, J. Phys. B **18**, 4511 (1985).
[45]K. Jung, Th. Antoni, R. Müller, K.-H. Kochum, and H. Ehrhardt, J. Phys. B **15**, 3535 (1982).